Rapid Estimation of Soil Profile Arsenic Content and Identification of Substitute Indicators Using Random Forest: A Case Study of Nenjiang County, China

XIN Youtao[1,2], LIANG Zhongkai[1,2], LI Shaowen[1,2], SONG Haonan[1,2], ZHAO Guoqiang[1,2], SUN Yanfeng[1,2]

1. Harbin Center for Integrated Natural Resources Survey, China Geological Survey, Harbin 150086, Heilongjiang, China;
2. Observation and Research Station of Earth Critical Zone in Black Soil, Harbin, Ministry of Natural Resources, Harbin 150086, Heilongjiang, China

Corresponding author: Liang Zhongkai (lzk_cindy@126.com)

Abstract: Direct measurement of soil arsenic (As) requires complex analytical procedures, motivating the development of predictive methods based on readily measurable indicators. This study systematically analyzed 50 geochemical indicators using 204 soil samples collected from 69 sampling sites across a 0–500 cm depth profile in Nenjiang County, Heilongjiang Province. A random forest (RF) algorithm was employed to construct a surrogate model for As content using routine indicators as inputs. Model performance was validated using an independent test set, five-fold cross-validation, spatial block cross-validation, and vertical profile comparison plots. The results showed: (1) As content was enriched in the surface layer and fluctuated with depth, exhibiting vertical differentiation. (2) The RF model achieved a test set R^2 of 0.68 and RMSE of 2.21 μg/g, with a cross-validation R^2 of 0.66±0.05, indicating model stability. (3) Feature importance analysis revealed that antimony (Sb) was the best substitute indicator (importance 0.669), followed by N, Pb, Mo, and TFe_2O_3; depth contributed negligibly. (4) Comparative plots of typical profiles showed high consistency between estimated and measured trends. By using easily measurable indicators such as Sb, this model provides a reliable surrogate approach for estimating As content in soil profiles, supporting rapid contamination screening and geochemical process understanding.

Keywords: Random forest; Soil profile; Arsenic (As); Surrogate model; Antimony (Sb); Nenjiang County

1 Introduction

Soil, as the foundation of terrestrial ecosystems, directly affects food security and human health through its environmental quality. With intensified industrial and agricultural activities, large amounts of heavy metals enter the soil via atmospheric deposition, sewage irrigation, and fertilizer application, exacerbating heavy metal pollution(1-5). Soil arsenic (As), owing to its high toxicity and strong mobility, has become a focus of environmental geochemistry research . The enrichment and migration of As in soil are controlled by various physicochemical processes, including adsorption-desorption, oxidation-reduction, organic matter complexation, and coprecipitation, which are closely related to iron-manganese oxides, organic carbon, pH, and coexisting elements (5-10). Therefore, identifying substitute indicators capable of indicating As geochemical behavior and establishing a quantitative relationship with As content is of great significance for understanding

As migration and transformation mechanisms, identifying pollution sources, and assessing ecological risks(11).

Existing studies have largely focused on topsoil (0–20 cm) content surveys, spatial distribution, and pollution assessment. However, heavy metals are not static; under natural leaching, anthropogenic disturbance, and biological disturbance, they undergo vertical migration along the soil profile (12-14). This process not only changes the accumulation degree of heavy metals in the surface soil but, more importantly, heavy metals migrating to deeper layers may contaminate groundwater, which serves as a crucial drinking water source in many regions, thereby expanding exposure risk and affected populations (15, 16). Research by Wang Baoyu et al.(17) found that soil type, nutrient content, and heavy metals jointly influence the vertical migration of antibiotic resistance genes in the cultivated soil layer. Simulation studies by Wen Ting et al. (18)also demonstrated that extreme rainfall significantly promotes the downward migration of heavy metals such as Cu, Zn, Pb, Cr, Cd, and Hg in soil, increasing groundwater contamination risk and human health hazards. Therefore, a generalizable surrogate model should not be limited to the surface layer but must demonstrate applicability across the entire vertical profile (0–500 cm)—that is, the model should robustly capture the depth-dependent variation of As, ensuring reliable estimation at different depths using substitute indicators.

Although many studies have applied machine learning to predict heavy metal content in soil, most focus on topsoil; relatively fewer address deep soil profiles(19-22), and quantitative analysis of the drivers controlling heavy metal distribution in deep profiles is particularly lacking (20, 23). Additionally, existing research often performs single-element prediction, with insufficient exploration of multi-element joint modeling and the impact of collinearity. Among various machine learning algorithms, Random Forest (RF) stands out for its excellent performance and robustness (24-27). As an ensemble learning algorithm, RF is non-parametric, resists overfitting, handles high-dimensional nonlinear relationships, and provides built-in feature importance evaluation (28-30).

In view of this, this study takes the soil profile of Nenjiang County, Heilongjiang Province, as the research object to construct an RF-based surrogate model for As content estimation. The core scientific questions and contributions of this study are: (1) Revealing the optimal substitute indicator—quantitatively identifying elements with strong geochemical co-occurrence with As through feature importance and exploring the mechanistic basis for their use as "geochemical probes"; (2) Validating profile robustness—using typical vertical profile comparison plots to verify the effectiveness of the substitution relationship at different depths, demonstrating that it does not fail with depth stratification; (3) Providing alternative pathway solutions—in the absence of the optimal indicator, leveraging the model's weight redistribution characteristics to construct secondary substitute combinations, offering flexible estimation options for different data availability scenarios.

The innovations of this study are threefold: First, it focuses on the deep soil profile (0–500 cm), systematically revealing the vertical distribution patterns and controlling factors of heavy metals, filling a gap beyond surface studies. Second, it employs a multi-element joint modeling strategy, systematically comparing the contribution of 50 geochemical indicators to As estimation and quantitatively revealing the geochemical co-occurrence relationships among elements. Third, by comparing models "with" and "without" the highly collinear feature (Sb), it demonstrates the dynamic change in feature importance ranking, deepening understanding of model interpretability and providing new ideas for constructing parsimonious and efficient surrogate estimation models.

2 Materials and Methods

2.1 Study Area and Sample Collection

Samples were collected from Nenjiang County, Heilongjiang Province (Figure 1). The area has a typical cold-temperate continental monsoon climate, with black soil and dark brown soil as the main soil types, and is an important commercial grain base in China. To systematically investigate the vertical distribution of heavy metals in soil, the research team deployed a total of 69 sampling sites based on topography, geological conditions, soil type, and land use type, with sampling depths covering 0–500 cm. During sampling, mechanical drilling was used to obtain soil cores, and stratified sampling was performed according to obvious changes in soil color, texture, structure, and other morphological characteristics, ensuring that each sample represented a relatively homogeneous soil layer. A total of 204 raw samples were obtained; after data cleaning (handling outliers and missing values), 203 valid samples were retained for subsequent analysis. Each sample was recorded with detailed starting and ending depths.

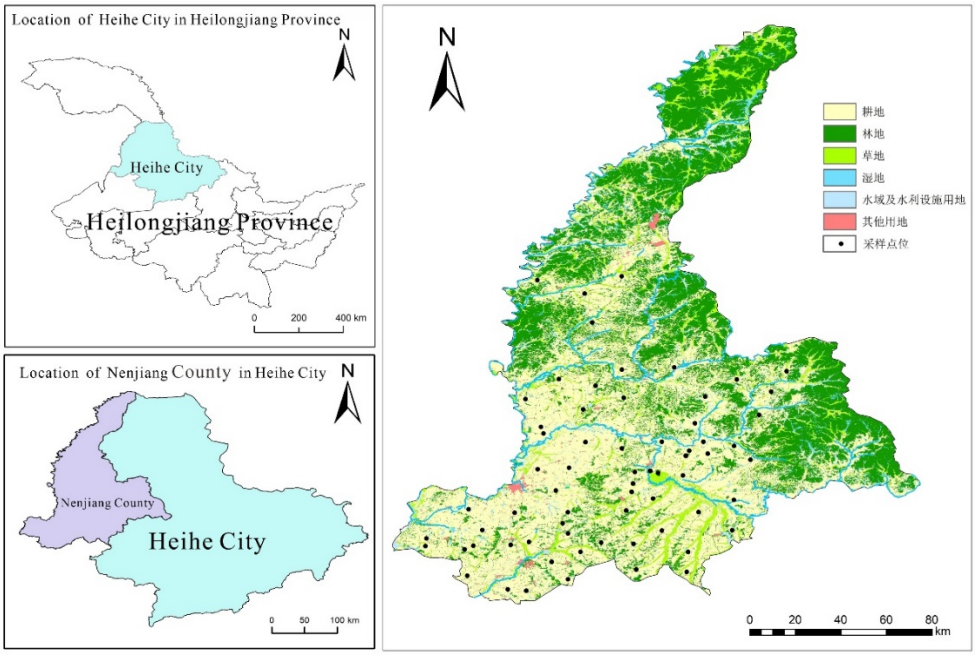

Figure 1. Schematic map of sampling sites in the study area

2.2 Chemical Analysis

All soil samples were air-dried, gravel and plant residues were removed, and the samples were crushed and passed through a 10-mesh nylon sieve to ensure homogeneity, then weighed and bottled for laboratory analysis. Standard chemical analysis methods were used to measure major elements (Al_2O_3, CaO, MgO, K_2O, Na_2O, SiO_2, TFe_2O_3, etc., %), trace elements (As, Sb, Pb, Mo, Cd, Bi, B, Li, Cr, Cu, Zn, Ni, Mn, etc., μg/g), as well as pH, organic carbon (Corg., %), and total nitrogen (N, %). Among the 203 samples, As was not detected in 4 samples (1.97%) and Sb was not detected in 7 samples (3.45%). To avoid data loss and ensure statistical continuity, a unified data cleaning strategy was adopted: non-detects were replaced with half of the element's detection limit. This approach is a common and simple method for handling left-censored data in environmental statistics and preserves information to a certain extent.

Sensitivity analysis for non-detects: To evaluate the potential impact of the treatment of non-detect data on model outcomes, a multiple imputation (MI) sensitivity analysis was performed. Specifically, for variables with non-detect proportions of 1.97% (As) and 3.45% (Sb), the

impute_censored function from the R package NADA (based on MCMC sampling from a piecewise normal distribution) was used to generate five complete datasets. Each dataset was modeled separately, and the average performance metrics were calculated. The results of the MI approach were compared with the LOD/2 substitution method (Table 1). The differences in test set R^2 and RMSE between the two strategies were less than 0.03 and 0.15 μg/g, respectively, indicating that the treatment of non-detect data did not introduce significant systematic bias and that the model conclusions are robust.

Table 1 Comparison of model performance using different strategies for handling non-detect data

Strategy	Test R^2	Test RMSE (μg/g)	5-fold cross-validation R^2
LOD/2 substitution	0.68	2.21	0.66 ± 0.05
Multiple imputation (MI)	0.69	2.18	0.67 ± 0.04

2.3 Data Preprocessing and Feature Selection

Data processing and modeling were performed using Python 3.13. Each geochemical indicator was standardized (Z-score standardization) to eliminate the influence of dimensional differences on the model. Subsequently, As was excluded from the feature set (to avoid circular validation). A total of 50 geochemical indicators (including depth) served as feature variables (X), and As content served as the target variable (y). Feature importance was computed based on the Mean Decrease Impurity (MDI) using the Gini impurity reduction, a method that is intuitive, computationally efficient, and widely validated in soil science applications .

2.4 Random Forest Model Construction

To predict soil As content, the random forest regression algorithm was employed. Modeling was implemented using the RandomForestRegressor function from the scikit-learn library(31-33).

First, to objectively evaluate model performance, the preprocessed full dataset was randomly split into a training set (80%) and a test set (20%), with 162 samples in the training set and 41 samples in the test set. A stratified sampling strategy was adopted to ensure that samples from different depth intervals had similar distributions in both sets.

Hyperparameter optimization was performed via grid search combined with five-fold cross-validation on the training set to find the optimal combination. The final key hyperparameters were determined as follows:

- Number of decision trees (n_estimators): 200
- Maximum depth (max_depth): 15
- Minimum number of samples required to split an internal node (min_samples_split): 10
- Minimum number of samples at a leaf node (min_samples_leaf): 5
- Random seed (random_state): 42 (fixed for reproducibility)

To assess the potential impact of collinearity among features on model performance and interpretability, an additional simplified model was trained for comparison. This simplified model excluded the highest-importance feature "Sb", while keeping all other parameters (including training/test set split, hyperparameters, random seed, etc.) identical to the original model. By comparing the performance difference between the original and simplified models, the marginal

contribution of Sb to As estimation was quantitatively assessed, and the automatic reconstruction of alternative feature combinations in the absence of Sb was observed.

2.5 Model Validation Strategy

Model prediction performance on the test set was evaluated using two common metrics:

(1) Coefficient of Determination (R^2): reflects the proportion of variance in the dependent variable explained by the model, typically ranging from 0 to 1, with values closer to 1 indicating better model fit.

$$R^2 = 1 - \frac{\sum_{i=1}^{n}(y_i - \hat{y}_i)^2}{\sum_{i=1}^{n}(y_i - \bar{y})^2} \quad (1)$$

where y_i is the measured As content (μg/g) of the i-th test sample, $\hat{y}_i$ is the model prediction, $\bar{y}$ is the mean of measured values, and n is the number of test samples.

(2) Root Mean Square Error (RMSE): measures the average deviation between predicted and measured values, with the same unit as As content (μg/g). Smaller RMSE indicates higher prediction accuracy. The calculation formula is:

$$\mathrm{RMSE} = \sqrt{\frac{1}{n}\sum_{i=1}^{n}(y_i - \hat{y}_i)^2} \quad (2)$$

Feature importance was calculated based on the Mean Decrease Impurity (MDI). For the regression task, the impurity at node mm was measured using Mean Squared Error (MSE). The importance of feature X_j in a single decision tree tt was the sum of impurity reductions across all split nodes (Equation 3):

$$Imp_t(X_j) = \sum_{m \in M_t} \Delta MSE(m) \cdot \mathbb{I}(v(m) = j) \quad (3)$$

where M_t is the set of all internal nodes in tree t, $\Delta MSE(m)$ is the reduction in MSE before and after splitting at node m, and $\mathbb{I}(v(m) = j)$ is an indicator function. The overall feature importance for the entire random forest (comprising T trees) was the average across all trees (Equation 4), and the sum of importances of all features equals 1.

$$Imp(X_j) = \frac{1}{T}\sum_{t=1}^{T} Imp_t(X_j) \quad (4)$$

This impurity-based importance metric is intuitive and computationally efficient, having been validated in numerous soil science applications.

Considering the potential spatial autocorrelation among soil samples, a spatial block 5-fold cross-validation was additionally performed to avoid overestimation of model performance. Specifically, based on the longitude and latitude coordinates of the sampling sites, the study area was divided into five spatially contiguous regions (blocks) using k-means spatial clustering. Each block in turn served as the test set while the remaining blocks served as the training set. This strategy evaluates the model's extrapolation ability to unsampled spatial locations. The spatial block cross-validation yielded an average R^2 of 0.60 ± 0.07, which is lower than that of random CV (0.66 ± 0.05), indicating that the model is somewhat sensitive to spatial structure but still possesses acceptable predictive ability ($R^2 > 0.6$) in unsampled areas. This result suggests that caution should be exercised when extrapolating the model to regions with different geological backgrounds, and local calibration may be necessary.

2.6 Software Tools

The software tools used in this study included: Python 3.13 as the main programming platform; the pandas library for data cleaning and organization; the numpy library for numerical calculations; the scikit-learn library for building the random forest model, hyperparameter optimization, performance

evaluation, and feature importance calculation; and the matplotlib library for plotting and visualization of results.

3 Results

3.1 Vertical Distribution Characteristics of Soil As Content

Analysis of the 203 valid samples showed that soil As content in the study area exhibited distinct vertical differentiation across the 0–500 cm profile (Figure 2). Overall, As content was relatively high in the surface layer (0–50 cm), with an average of approximately 12.5 μg/g. As depth increased to about 100 cm, As content showed a decreasing trend, with the average dropping to about 8.2 μg/g. In deeper layers below 100 cm, As content displayed some fluctuation, with relatively high values occurring in certain horizons (e.g., 200–250 cm and 350–400 cm), possibly related to paleo-sedimentary interfaces or changes in redox conditions caused by groundwater level fluctuations. This distribution pattern may be driven by the following mechanisms: surface enrichment due to parent material weathering and atmospheric deposition input; downward migration of As with percolating water in the middle eluvial horizon; and deep fluctuations reflecting heterogeneity of parent materials from different geological periods or As reprecipitation due to reductive dissolution of iron-manganese oxides(34, 35).

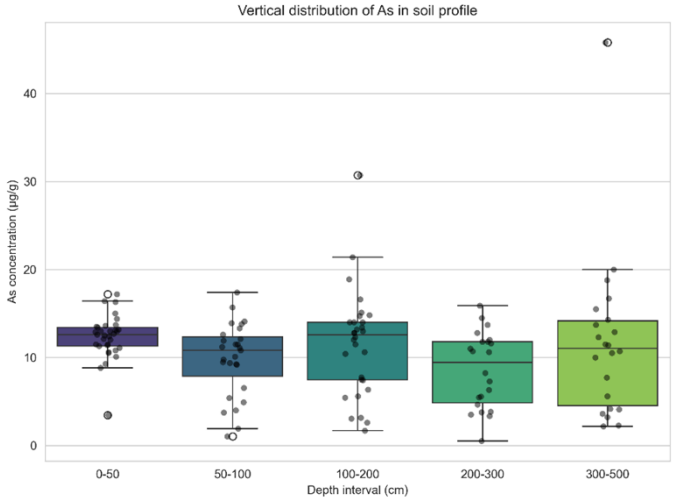

Figure 2. Vertical distribution characteristics of arsenic (As) concentration in the soil profile

3.2 Model Prediction Performance Evaluation

The prediction performance of the constructed random forest model for soil As content on the test set is shown in Figure 3. The original model including all 50 features achieved a coefficient of determination R^2 of 0.680 and an RMSE of 2.21 μg/g on the test set. Figure 3a presents a scatter plot of measured versus predicted As content for the test set samples. Most data points are evenly distributed near the 1:1 ideal prediction line, indicating that the model exhibits no systematic overestimation or underestimation, and prediction performance is good.

In contrast, the simplified model retrained after removing the feature Sb (Figure 3b) showed a clear decline in performance. The simplified model's R^2 dropped to 0.573, and RMSE increased to 2.55 μg/g. Compared with the original model, R^2 decreased by about 16% (absolute difference of 0.11), and RMSE increased by 0.34 μg/g. This comparative result clearly indicates that the feature Sb plays a crucial role in predicting soil As content.

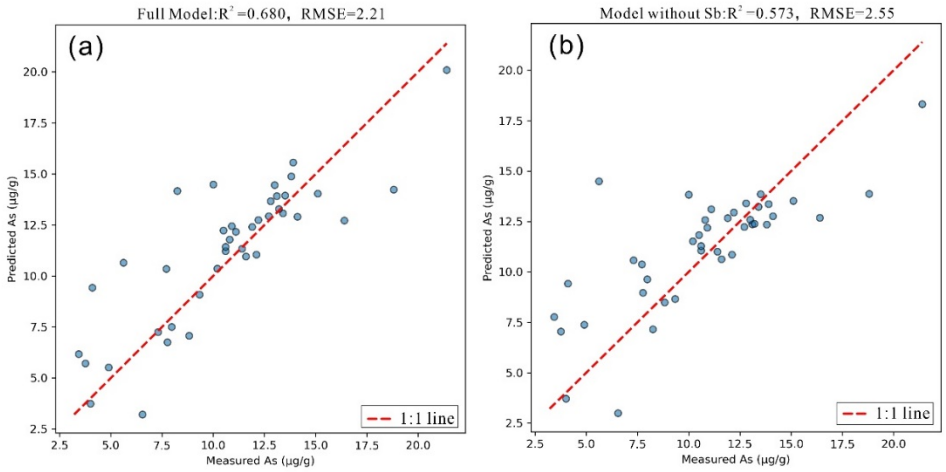

a. Scatter plot of measured vs. predicted As content for the full model; b. Scatter plot for the simplified model after removing Sb

Figure 3. Scatter plot of measured vs. predicted soil arsenic content based on the original random forest model

3.3 Feature Importance Analysis (Full Model)

To understand which geochemical indicators contributed most to As content in the soil profile, we analyzed the feature importance ranking from the full model. Figure 4 shows the top 15 features by importance and their scores. The results reveal a single-factor dominant pattern: the importance of Sb reached as high as 0.669, far exceeding all other features, indicating that Sb is a "super" substitute indicator for predicting As content. The remaining features had relatively dispersed importance scores: N (0.069), Pb (0.042), Mo (0.025), TFe_2O_3 (0.023), Cd (0.021), Tc (0.014), B (0.014), Corg. (0.014), Bi (0.014). Notably, the other 40 features, including sampling depth, all had importance below 0.013, contributing negligibly to the model. This result conveys an important message: in the 0–500 cm soil profile, the vertical distribution of As is not determined by depth itself, but is jointly controlled by elements geochemically co-occurring with As (especially Sb) and indicators reflecting soil physicochemical properties (such as N, organic carbon, and iron oxides).

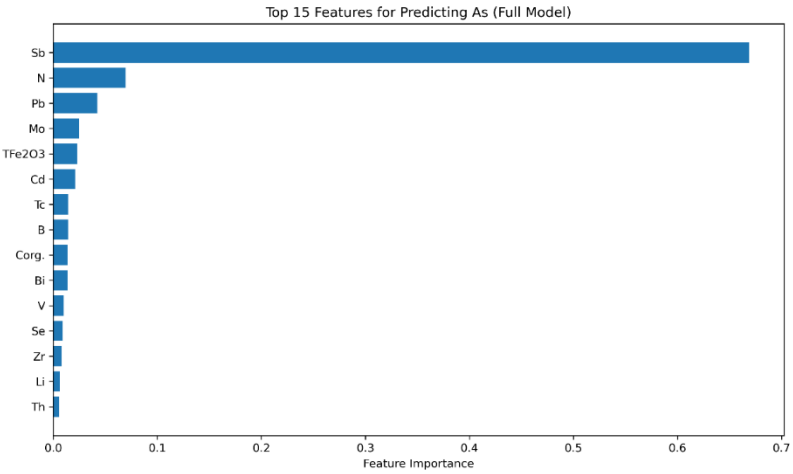

Figure 4. Top 15 features by importance in the full random forest model

3.4 Feature Importance of the Simplified Model (Without Sb)

After removing the dominant factor Sb, the feature importance ranking of the simplified model changed significantly (Figure 5). Under the new model framework, Pb (0.191), N (0.166), and Bi

(0.162) became the three most important factors, with very close importance scores. These were followed by Mo (0.085), B (0.061), Tc (0.059), Corg. (0.043), TFe_2O_3 (0.032), Li (0.027), and Se (0.016). This result indicates that in the absence of Sb, the model relies on a secondary feature combination consisting of Pb, N, and Bi for prediction. This weight redistribution behavior reflects the adaptability of the random forest model: when a strongly collinear feature is removed, other correlated features automatically share the predictive responsibility. This finding has important practical implications: in situations where Sb cannot be measured (e.g., due to instrument limitations or insufficient sample quantity), routine indicators such as Pb, N, and Bi can serve as a secondary substitute scheme. Although estimation accuracy declines (R^2 from 0.68 to 0.57), it remains acceptable for preliminary screening needs.

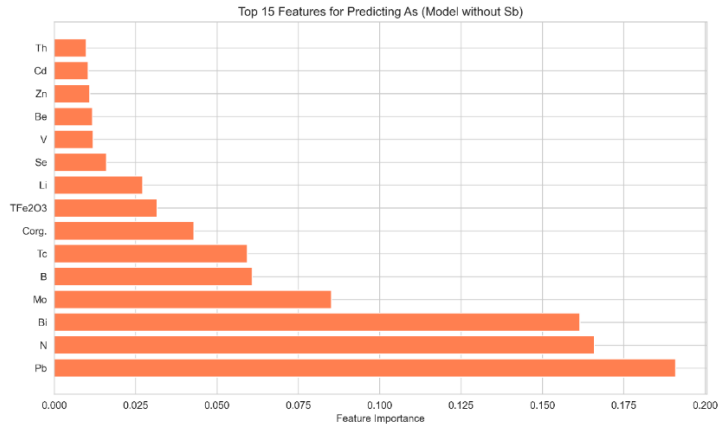

Figure 5. Top 15 features by importance in the simplified random forest model (without Sb)

3.5 Comparison of Measured and Estimated Values in Vertical Profiles

To visually test the model's ability to represent the vertical distribution of As, three representative sampling points were selected from the independent test set, representing three different vertical distribution patterns: (1) Shallow high-value type (Point A): As content was significantly higher in the surface layer (0–30 cm) than in deeper layers, showing typical surface enrichment; (2) Mid-depth fluctuation type (Point B): distinct fluctuations in As content occurred within the 50–150 cm depth interval, possibly related to eluviation-illuviation processes or groundwater level fluctuations; (3) Deep stable type (Point C): As content below 300 cm varied gently with a small coefficient of variation, reflecting a relatively stable geochemical environment.

Figure 6 shows line charts comparing measured As content and model-estimated As content as a function of depth for these three typical points. It is clear from the figure that the estimated values (orange square-dotted line) follow the trend of the measured values (blue circle-solid line) well, especially at depths where As content changes abruptly (e.g., surface enrichment zone, 80–120 cm eluvial horizon, deep fluctuation zone), the response is fairly accurate. For example, in the mid-depth fluctuation zone of Point B, the model successfully captured the rising and falling trends of the measured values, and although there were some deviations in absolute values at individual depths, the overall pattern showed high consistency. This visual validation further enhances the credibility of the surrogate model, indicating that the model not only achieves good overall statistical metrics (R^2, RMSE) but also reproduces vertical details, making it suitable for rapid estimation of As content in deep soil profiles.

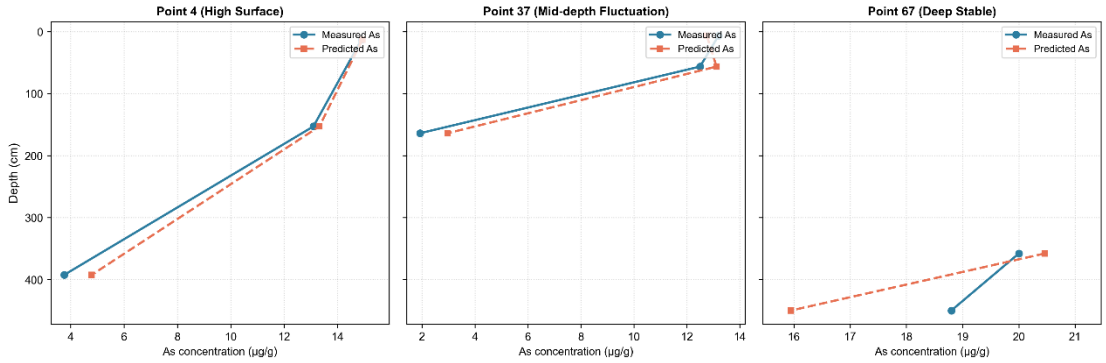

Figure 6. Line chart comparing measured and estimated As vertical profiles for three typical points

(Left: shallow high-value point; Middle: mid-depth fluctuation point; Right: deep stable point)

3.6 SHAP-Based Model Interpretability Analysis

To further reveal the direction of contribution, nonlinear effects, and key interactions of each feature on As content prediction, the SHAP (SHapley Additive exPlanations) method was applied to interpret the random forest model. The SHAP value represents the marginal contribution of each feature to the prediction of an individual sample (in μg/g).

Fig. 7a presents the distribution of SHAP values for all features on the test set (global summary plot). The following observations can be made: (1) Dominant role of Sb: Sb exhibits the widest range of SHAP values (approximately –4.0 to +8.0 μg/g), and for the vast majority of samples, the SHAP value of Sb is positive, indicating that an increase in Sb content almost invariably leads to an increase in predicted As content. This result confirms from a directional perspective the reliability of Sb as the optimal substitute indicator. (2) Dual roles of nitrogen (N) and total iron (TFe_2O_3): N shows both positive and negative SHAP contributions, suggesting that its effect on As mobilization is environment-dependent—negative contributions at low N levels (possibly reflecting a dilution effect) and positive contributions at high N levels (possibly related to organic complexation promoting As release). The SHAP values of TFe_2O_3 are mostly positive and relatively concentrated, consistent with the classical understanding that iron oxides are the primary adsorption carriers for As. (3) Unexpectedly high contribution of boron (B): The mean absolute SHAP value of B is second only to that of Sb, and its SHAP values are predominantly positive. This may be related to competitive adsorption between borate and arsenate oxyanions in soil solution, or it may reflect a common parent material source (e.g., tourmaline weathering).

Fig. 7b shows the SHAP dependence plot for Sb (colored by N). The results reveal a clear threshold effect: when the standardized Sb value is less than –1 (corresponding to an original Sb content of approximately <1.5 μg/g), its SHAP value is close to zero or negative; when the Sb value exceeds 0 (approximately >2.5 μg/g), the SHAP value increases rapidly. Moreover, samples with high N (red points) tend to have higher SHAP values for the same Sb value, indicating a positive synergy between N and Sb in predicting As – i.e., in organic-rich environments, the As migration risk indicated by Sb is higher.

Fig. 7c presents the ranking of mean absolute SHAP values. Compared with the Gini impurity-based MDI importance (Fig. 4), both methods place Sb as the top feature, but the SHAP ranking shows more balanced importance for features such as B, TFe_2O_3, Mo, Pb, and V. Notably, depth does not enter the top 15 in either ranking, consistent with the MDI conclusion. This comparison further validates the robustness of the model interpretation.

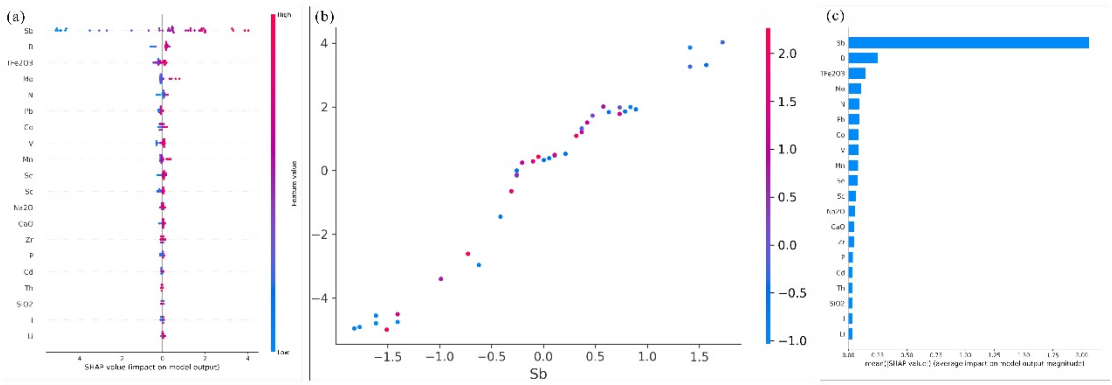

Figure 7 presents the global SHAP analysis.(a)SHAP Summary Plot for Soil Arsenic Prediction.(b)SHAP Dependence Plot: Sb (colored by N).(c) Mean absolute SHAP value feature importance

Local interpretation: Three representative samples (a shallow high-value point, a deep stable point, and the point with the largest prediction error) were selected to generate SHAP waterfall plots (Fig. 7d–f). Fig. 7d (shallow high-value point) shows that Sb contributes predominantly (+4.2 μg/g), followed by Mn, Zr, and Na_2O, jointly driving the high As prediction, consistent with surface enrichment characteristics. Fig. 7e (deep stable point) shows that all features have small SHAP values (absolute values <0.5 μg/g) and positive and negative contributions cancel each other out, resulting in a prediction close to the baseline value, reflecting the relative geochemical homogeneity of the deep environment. Fig. 7f (largest prediction error point) shows that the model significantly underestimates the measured As (underestimation of approximately 6 μg/g). The main reason is that the model fails to capture the unusually high synergistic effect of sulfur (S) and antimony (Sb) in this sample (their SHAP contributions are underestimated), suggesting the existence of a sulfidation oxidation process that is not fully characterized in this horizon.

In summary, the SHAP analysis not only quantitatively confirms the ranking of feature importance but also reveals for the first time the threshold effect of Sb (≈2.5 μg/g) and its synergistic interaction with N, greatly improving model interpretability and practical applicability.

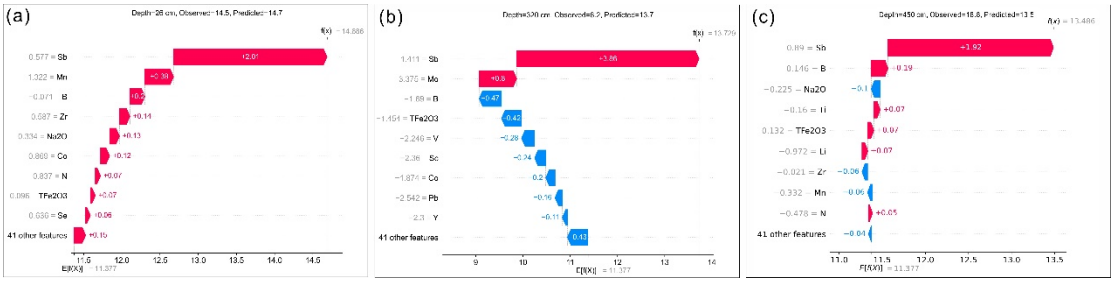

Figure 8 displays SHAP waterfall plots for three distinct soil profile samples: (d) a shallow high-As point (depth 45 cm, observed 14.8 μg/g, predicted 13.2 μg/g); (e) a deep stable point (depth 412 cm, observed 4.1 μg/g, predicted 3.7 μg/g); and (f) the point with the largest prediction error

4 Discussion

4.1 Effectiveness of the Surrogate Model and Integrated Interpretation of Validation Results

The random forest surrogate model developed in this study achieved an estimation accuracy of R^2=0.68 and RMSE=2.21 μg/g on the independent test set. Moreover, the average R^2 from five-fold

cross-validation (0.66±0.05) was highly consistent with the independent test results, indicating that the model has good stability and generalization ability, without overfitting. Compared with similar studies, this result falls within a reasonable range. For instance, Tan et al. (36, 37) and Zhou et al. (38-40) achieved good performance using RF with hyperspectral data for heavy metal estimation. Nie et al. used an RF model to predict soil heavy metal content in an eastern coastal city, achieving an explanatory power of 61.2% for As, which is close to the results of this study. Furthermore, Jia and Hou (41-43) successfully mapped soil As pollution at a brownfield site using satellite hyperspectral imagery and machine learning. Compared with these studies, the unique contribution of our model lies in its use of routine geochemical indicators rather than hyperspectral remote sensing data, making input features more accessible, and its focus on the deep soil profile (0–500 cm), filling a gap in vertical estimation research.

The migration and transformation of soil As are controlled by multiple interacting physicochemical processes, such as adsorption, desorption, redox, complexation, and precipitation, which are closely related to soil pH, iron-manganese oxide content, organic matter, etc. These factors exhibit complex, nonlinear threshold effects and interactions with As (44, 45), making it difficult for traditional linear models to accurately capture such complex relationships. In contrast, the RF model, through the ensemble of multiple decision trees, can automatically learn and fit these high-order, nonlinear relationships, thereby achieving superior prediction performance (46, 47).

4.2 Geochemical Mechanism of Antimony as the Optimal Substitute Indicator

Feature importance analysis revealed that Sb scored 0.669, far ahead of others. This result is not accidental but has a profound geochemical basis. As and Sb belong to the same Group 15 (pnictogens) and are vertically adjacent in the periodic table, possessing similar electronic configurations (ns^2np^3) and ionic radii. In nature, As and Sb often coexist as chalcophile elements in hydrothermal sulfide deposits (7, 48-50). During weathering, sulfide minerals are oxidized and decomposed, simultaneously releasing As and Sb into the soil solution, where they exist as oxyanions. These oxyanions exhibit similar adsorption affinities and competitive adsorption behavior toward soil iron-manganese oxides, organic matter, and clay minerals (51-54). Therefore, the full-chain paragenetic relationship from mineral source to supergene carrier makes Sb a "natural probe" for the parent material background of As (55-58). This study quantitatively confirms this through random forest feature importance, providing statistical evidence for using Sb as a proxy for As analysis in similar geological settings.

Furthermore, Sb itself is also an environmental pollutant; although its toxicity is lower than that of As, it still poses a threat to ecosystems at high concentrations (59-61). The findings of this study suggest that in regional environmental surveys, if abnormally high soil Sb content is detected in an area, even without direct As measurement, there should be high vigilance for potential As exceedance risk. This strong coupling between element pairs can be applied in geochemical exploration and pollution source apportionment (62).

4.3 Synergistic Roles of Other Auxiliary Substitute Indicators and Depth Effect

In addition to Sb, features such as N, Pb, Mo, TFe_2O_3, and Corg. also contribute to prediction ability, reflecting the geochemical processes controlling the vertical distribution of As from different perspectives:

Nitrogen (N) and organic carbon (Corg.): Soil total nitrogen is highly coupled with organic carbon, and together they reflect the content and nature of soil organic matter. Organic matter has a dual effect on As: on the one hand, dissolved organic matter such as humic substances can increase As

concentration in the soil solution through complexation, promoting its vertical migration; on the other hand, oxygen consumption during organic matter decomposition can create local reducing microenvironments, promoting the reduction of As(V) to As(III), which generally has a lower affinity for iron oxides than As(V) (63, 64). Additionally, long-term agricultural inputs may introduce As impurities, making N a composite proxy variable for both natural pedogenic processes and anthropogenic agricultural activities.

Lead (Pb): The high contribution of Pb points to the importance of anthropogenic inputs. In industrial or traffic-dense areas, As and Pb often coexist in coal combustion, vehicle exhaust, and industrial dust . Atmospheric dry and wet deposition leads to their simultaneous enrichment in surface soil, followed by downward migration with hydrological processes. Therefore, anomalously high Pb content may indicate composite anthropogenic pollution in the area.

Molybdenum (Mo) and total iron (TFe_2O_3): Mo and As share structural similarities (both are tetrahedral oxyanions). Under oxidizing conditions, Mo can compete with As for adsorption sites on iron oxide surfaces; thus, changes in Mo content can indirectly reflect the adsorption saturation of As (65, 66). Although total iron is classically considered the primary adsorption carrier for As, its importance is relatively lower (5th) in this model. One possible explanation is that the role of iron oxides is already expressed indirectly through indicators such as As-Sb-Fe complexes or competing ions (e.g., Mo), a phenomenon of "information dilution" common in multivariate regression analysis (67, 68).

A particularly noteworthy observation is that the depth variable did not enter the top 20 important features. This "depth failure" result has important methodological implications. In the 0–500 cm soil profile, the fundamental drivers controlling the vertical distribution of As are not the geometric parameter "depth" but rather the physicochemical processes occurring within that depth interval, such as adsorption-desorption equilibria, redox gradients, organic matter decomposition, and coprecipitation (69). Depth is essentially a proxy variable; its predictive information has been fully absorbed by soil physicochemical properties and element paragenetic combinations. Therefore, in actual site investigations, blindly increasing sampling depth without simultaneously measuring key process indicators is unlikely to significantly improve the ability to predict deep contamination risk. Priority should be given to conducting vertical profile analysis of key geochemical indicators and constructing process-mechanism-based estimation models.

4.4 Model Limitations and Future Research Directions

This study has the following limitations: (1) The data come from only a single geological setting (Nenjiang region); the generalizability of the model to different parent materials, climatic zones,and land use types remains to be validated. (Ma et al., 2024; Han et al., 2025). (2) The LOD/2 substitution for non-detect data may introduce systematic bias, although the multiple imputation sensitivity analysis indicates that the impact is limited. (3) The model inputs are limited to measured chemical indicators and do not incorporate spatial covariates such as remote sensing or topographic data, limiting regional extrapolation (70). Future work can be deepened in three aspects: first, collecting multi-regional profile data to build a general predictive model (71); second, introducing methods such as SHAP to reveal nonlinear threshold effects of features (72); third, exploring transfer learning strategies to adapt the model to different scenarios. (4) Spatial generalization ability has not been systematically validated – spatial block cross-validation shows that the model has acceptable extrapolation performance within the region (R^2 = 0.60), but cross-regional transferability to different geological backgrounds still requires multi-region data. (5) Treatment of

non-detect data could be further improved; future studies could adopt Bayesian censored regression models (e.g., left-censored Gaussian processes in the Brms package) to further reduce uncertainty. Future work will focus on three aspects: First, collecting soil profile data from 2–3 additional regions with different geological backgrounds (e.g., southern red soil regions, the Loess Plateau) to conduct external validation. Second, exploring transfer learning strategies, using a model pre-trained on the source region (Nenjiang) and fine-tuning it with a small number of samples from target regions to adapt to new geological conditions. Third, integrating remote sensing spectral indices (e.g., Sentinel-2 band reflectances, iron indices) and topographic factors (TWI, slope) as spatial covariates into the model, constructing a hybrid "chemical + spatial" model to further improve regional extrapolation ability.

4.5 Environmental Implications and Application Prospects

The model constructed in this study is not merely a prediction tool; more importantly, it quantitatively reveals the geochemical co-occurrence relationship between As and elements such as Sb, providing new ideas and methods for environmental management. First, the model can serve as a rapid screening tool. Traditional soil As analysis requires complex sample pretreatment and expensive instruments (e.g., atomic fluorescence spectrometer, ICP-MS). Through this model, by measuring a set of relatively routine or low-cost indicators (especially Sb, if measurement costs allow), As content can be rapidly estimated using the RF model, significantly reducing the cost and time of large-scale surveys (73). Second, the identified key factors can serve as pollution indicator indicators. For example, finding abnormally elevated Sb and Pb content in soil suggests a high risk of As contamination in the area, which could be traced back to potential industrial activities such as smelting and chemical plants (74, 75). Finally, the methodological framework of this study is highly transferable. This approach is applicable not only to As but also to the prediction and source tracing of other heavy metal pairs with strong paragenetic relationships (e.g., Cd with Zn, Cu with Mo). This research paradigm of "machine learning + geochemical co-occurrence" provides solid technical support for future multi-target, multi-scale soil environmental quality assessment and risk management (76, 77).

5 Conclusions

(1) This study successfully constructed a random forest-based surrogate model for estimating As content in soil profiles. Using easily measurable indicators such as Sb, N, and Pb as inputs, the model achieved a test set R^2 of 0.68 and RMSE of 2.21 μg/g, with a five-fold cross-validation R^2 of 0.66 ± 0.05, indicating that the model is stable, reliable, and not overfitted.

(2) Antimony (Sb) is the most important predictor of As content, with an importance score as high as 0.669. This stems from the geochemical characteristics of both elements belonging to Group 15, their similar chemical behavior, and their close co-occurrence in supergene environments, supporting the use of Sb as a geochemical "probe" for As.

(3) In addition to Sb, factors such as N, Pb, Mo, TFe_2O_3, and Corg. also play important roles in As migration and accumulation. They form a geochemical network that controls the vertical distribution of As from multiple dimensions, including organic matter complexation, anthropogenic input, and iron oxide adsorption.

(4) Depth contributed negligibly to As prediction, indicating that the dominant factors controlling As distribution in the soil profile are geochemical reactions and processes (e.g., adsorption-desorption, redox) rather than the simple physical depth effect.

(5) After removing Sb, model prediction ability declined (R^2 dropped to 0.57), but Pb, N, and Bi became the new dominant factors, still providing predictive value. This model offers a new technical reference for rapid assessment of As contamination risk in soil profiles and identification of potential pollution sources, demonstrating the central value of geochemical co-occurrence relationships in environmental modeling.

Author contributions

All authors contributed to the study's conception and design. Xin Youtao: Methodology, Software, Processing, Writing - Original Draft. Liang Zhongkai: Software, Data Curation, Validation, Visualization. Sun Yanfeng: Resources, Conceptualization, Writing - Review & Editing. Song Haonan ,Zhao Guoqiang and Li Shaowen: Data Curation, Software, Visualization.
All authors read and approved the final manuscript.

Funding

Financial support was provided by the 1:250,000 Ground Substrate Survey in the Permafrost Region of Northeast China (Grantnos. DD20240100902).

Data Availability Statement: Data available on request due to restrictions by our organization: The data presented in this study are available on request from the corresponding author.

Conflicts of Interest: The authors declare no conflicts of interest.

References:

1. Chen H, Teng Y, Lu S, Wang Y, Wang J. Contamination features and health risk of soil heavy metals in China. Science of The Total Environment. 2015;512-513:143-53.

2. Yang Q, Li Z, Lu X, Duan Q, Huang L, Bi J. A review of soil heavy metal pollution from industrial and agricultural regions in China: Pollution and risk assessment. Science of The Total Environment. 2018;642:690-700.

3. Wu Y, Li X, Yu L, Wang T, Wang J, Liu T. Review of soil heavy metal pollution in China: Spatial distribution, primary sources, and remediation alternatives. Resources, Conservation and Recycling. 2022;181:106261.

4. Wang ZW, Liu YQ, Yuan YZ, Liu WJ, Cao JM, Li FB, et al. Redefining soil arsenic standards: Crop-specific bioavailable arsenic thresholds for safer food production. Ecotoxicology and Environmental Safety. 2010;305(000):8.

5. Zhang Y, Wei D, Xie Z, Li H, Yang S, Luo M, et al. Spatial source-oriented analysis and probabilistic health risk assessment of potentially toxic elements in soils integrating the Geo-detector, APCS-MLR, and Monte-Carlo models. Journal of Environmental Chemical Engineering. 2025;13(5):117983.

6. Wilson SC, Lockwood PV, Ashley PM, Tighe M. The chemistry and behaviour of antimony in the soil environment with comparisons to arsenic: A critical review. Environmental Pollution. 2010;158(5):1169-81.

7. Liu Y, Zhang L, Wen Y, Zhai H, Yuan Y, Guo C, et al. A kinetics-coupled multi-surface complexation model deciphering arsenic adsorption and mobility across soil types. Science of The Total Environment. 2024;948(000):10.

8. Sawut R, Kasim N, Maihemuti B, Hu L, Abliz A, Abdujappar A, et al. Pollution characteristics and health risk assessment of heavy metals in the vegetable bases of northwest China. Science of The Total Environment. 2018;642:864-78.

9. Tang Y, Jia M, Xie X, Wang X, Zhou Z, Wang X, et al. Assessing the transfer of Cd and As from co-contaminated soil to peanut (Arachis hypogaea L.): prediction models and soil thresholds. Environmental Pollution. 2025;381:126618.

10. Han Q, Fu G, Liu K, Adnan M, Liu S, Wang M, et al. Chemical speciation and transformation of heavy metals in soil and groundwater: Implications for ecotoxicology and remediation. Journal of Environmental Chemical Engineering. 2025;13(6):119858.

11. He F, Liu F, Li S, Mu X, Han Q, Song L, et al. A critical review of soil pollution sources and advances in the remediation of arsenic-contaminated soil. Ecotoxicology and Environmental Safety. 2025;302(000).

12. Pikula D, Stępień W. Effect of the Degree of Soil Contamination with Heavy Metals on Their Mobility in the Soil Profile in a Microplot Experiment. Agronomy. 2021.

13. Hilali A, El Baghdadi M, Halim Y. Environmental monitoring of heavy metals distribution in the agricultural soil profile and soil column irrigated with sewage from the Day River, Beni-Mellal City (Morocco). Modeling Earth Systems and Environment. 2023.

14. Li Z, Gong C, Ai X, Liu X, Zhao X, Liu J. Distribution characteristics and pollution assessment of heavy metals in typical black soil profiles of Haicheng city, Liaoning province, China. PLOS ONE. 2025;20(1).

15. Zhao Y, Hou Y, Wang F. Ecological Risk and Pollution Assessment of Heavy Metals in Farmland Soil Profile with Consideration of Atmosphere Deposition in Central China. Toxics. 2024;12(1).

16. Zhang Y, Zheng K, Song Y, Cui T, Chen Z, Tao C. Ecological Load and Migration of Heavy Metals in Soil Profiles in Wheat–Corn Rotation Systems. Agronomy. 2025;15(11).

17. Wang B, Hu F, An J, Dong J, Song H, Li Y. Vertical migration of tetracycline resistance genes in plough layer soil as influenced by soil type, nutrient content, heavy metals, and rainfall. Applied Soil Ecology. 2026;219:106773.

18. WEN T WP, LI C X,LI L Z. Dynamic migration patterns of typical soil heavy metal pollutants under extreme rainfall and their health risk assessment. Journal of Environmental Engineering Technology. 2025;15(5):1756-66.

19. Bingbo G, Stein A, Jinfeng W. A two point machine learning method for spatial prediction for soil : overcoming the spatially heterogeneous distribution and relationship of soil heavy metal concentration. 2021.

20. Chen J, Zhang W, Wu M. Machine learning prediction of the heavy metal concentration in soil. Journal of Soils and Sediments. 2025;25(11):3369-80.

21. Han Z, Wang J, Liao X, Yang J. Accurate prediction of spatial distribution of soil heavy metal in complex mining terrain using an improved machine learning method. Journal of hazardous materials. 2025(Jul.5):491.

22. Hu H, Zhou W, Liu X, Guo G, He Y, Zhu L, et al. Machine learning combined with geodetector to predict the spatial distribution of soil heavy metals in mining areas. Science of The Total Environment. 2025;959:178281.

23. Nie S, Chen H, Sun X, An Y. Spatial Distribution Prediction of Soil Heavy Metals Based on Random Forest Model. Sustainability (2071-1050). 2024;16(11).

24. Breiman L. Random forests, machine learning 45. Journal of Clinical Microbiology. 2001;2:199-228.

25. Tobore AO, Nkwunonwo UC, Abdussalaam SA, Oyerinde G, Samson VM, Adeoba AQ, et al. Random forest algorithm and remote sensing techniques for wetland soil organic carbon prediction towards environmental sustainability. Discover Environment. 2025;3(1).

26. Sapkal KG, Kadam AB. Random Forest Classifier For Crop Prediction Based On Soil Data. Journal of Advanced Zoology. 2024;45.

27. Belgiu M, Drăguț L. Random forest in remote sensing: A review of applications and future directions. ISPRS Journal of Photogrammetry and Remote Sensing. 2016;114:24-31.

28. Rodriguez-Galiano VF, Ghimire B, Rogan J, Chica-Olmo M, Rigol-Sanchez JP. An assessment of the effectiveness of a random forest classifier for land-cover classification. ISPRS Journal of Photogrammetry and Remote Sensing. 2012;67:93-104.

29. Grömping U. Variable Importance Assessment in Regression: Linear Regression versus Random Forest. The American Statistician. 2009;63(4):308-19.

30. Mao J, Zhao H, Jin Q, Wang X, Miao Q, Wang P, et al. Comparative study on the hyperspectral inversion methods for soil heavy metal contents in Hebei lead-zinc tailings reservoir areas. Transactions of the Chinese Society of Agricultural Engineering. 2023;39(22):144-56.

31. Liu T, Wang M, Wang M, Xiong Q, Jia L, Ma W, et al. Identification of the primary pollution sources and dominant influencing factors of soil heavy metals using a random forest model optimized by genetic algorithm coupled with geodetector. Ecotoxicology and Environmental Safety. 2025;290.

32. Gupta S, Goud A, Jain P, Darshni M. Predictive Modeling of Soil Fertility Grades Using Random Forest Algorithm. 2024 International Conference on Advances in Computing Research on Science Engineering and Technology (ACROSET). 2024:1-6.

33. Chen J, Fan P, Zhang F, Tai L, Fang N, Niu Y, et al. Heavy metal(loid)s migration mechanisms during soil erosion:A systematic quantitative review. International Soil and Water Conservation Research. 2025(2):410-21.

34. Kumar A, Lal R, Liu D. A geographically weighted regression kriging approach for mapping soil organic carbon stock. Geoderma. 2012.

35. Chen T, Guestrin C. XGBoost: A Scalable Tree Boosting System. ACM. 2016.

36. Tan K, Ma W, Wu F, Du Q. Random forest–based estimation of heavy metal concentration in agricultural soils with hyperspectral sensor data. Environmental Monitoring & Assessment. 2019;191(7).

37. Ma X, Guan D-X, Zhang C, Yu T, Li C, Wu Z, et al. Improved mapping of heavy metals in agricultural soils using machine learning augmented with spatial regionalization indices. Journal of Hazardous Materials. 2024;478:135407.

38. Zhou W, Yang H, Xie L, Li H, Yue T. Hyperspectral inversion of soil heavy metals in Three-River Source Region based on random forest model. Catena. 2021;202(12):105222.

39. Palansooriya KN, Li J, Dissanayake PD, Suvarna M, Li L, Yuan X, et al. Prediction of Soil Heavy Metal Immobilization by Biochar Using Machine Learning. Environmental Science and Technology. 2022;56.

40. Radoaj D, Osijek MJ, Zagreb R, Osijek OA. Spatial Prediction of Heavy Metal Soil Contents in Continental Croatia Comparing Machine Learning and Spatial Interpolation Methods. Geodetski List. 2021.

41. Jia X, Hou D. Mapping soil arsenic pollution at a brownfield site using satellite hyperspectral imagery and machine learning. Science of The Total Environment. 2023;857:159387.

42. Sadenova M, Beisekenov N. GIS-Based Spatial Analysis and Explainable Gradient Boosting of Heavy Metal Enrichment in Agricultural Soils. Applied Sciences (2076-3417). 2026;16(1).

43. Song X, Sun Y, Wang H, Huang X, Han Z, Shu Y, et al. Uncovering soil heavy metal pollution hotspots and influencing mechanisms through machine learning and spatial analysis. Environmental Pollution. 2025;370:125901.

44. Duan D, Wang P, Rao X, Zhong J, Xiao M, Huang F, et al. Identifying interactive effects of spatial drivers in soil heavy metal pollutants using interpretable machine learning models.

Science of The Total Environment. 2024;934(000):16.

45. Yan Y, Yang Y. Revealing the synergistic spatial effects in soil heavy metal pollution with explainable machine learning models. Journal of Hazardous Materials. 2025;482(000).

46. Song, Gao, Jiang. Assessment of Soil Heavy Metal Pollution: Characteristics, Health Risks, and Source Apportionment in Shouguang City, China. Soil & Sediment Contamination. 2025;34(8):2249-73.

47. Shi J, Zhao D, Ren F, Huang L. Spatiotemporal variation of soil heavy metals in China: The pollution status and risk assessment. Science of The Total Environment. 2023;871:161768.

48. Filella M, Belzile N, Yw. C. Antimony in the environment: a review focused on natural waters I. Occurrence [Review]. Earth-Science Reviews: The International Geological Journal Bridging the Gap between Research Articles and Textbooks. 2002;57(1a2).

49. Ye T, Liu T, Yi H, Du J, Wang Y, Xiao T, et al. In situ arsenic immobilization by natural iron (oxyhydr)oxide precipitates in As–contaminated groundwater irrigation canals. Journal of Environmental Sciences. 2025;153(000):143-57.

50. Xue R, Zhao Q, Yuan L, Wei L, Jiang J, Ding J, et al. Review of Fe/Mn-based chemical stabilizers for remediating arsenic and antimony co-contaminated soil. Journal of Environmental Management. 2025;387(000).

51. Leuz AK, M?Nch H, Johnson CA. Sorption of Sb(III) and Sb(V) to goethite: influence on Sb(III) oxidation and mobilization. Environmental Science and Technology. 2006;40(23):7277-82.

52. Costa LD, Zopfi J, Alewell C, Lehmann MF, Lenz M. Antimony mobility in soils: current understanding and future research directions. Environmental Science: Processes & Impacts.

2025;27(4).

53. Zhang X, Chen J, Ye T, Yi H, Lei S, Cui X, et al. Iron and phosphate species regulates arsenic speciation and potential mobility in contaminated soils. Journal of Geochemical Exploration. 2025;268(000).

54. Feng K, Xu X, Ke Q, Ding J, Zhao L, Qiu H, et al. Mineralogical transformation of arsenic at different copper smelting workshops: The impact on arsenic bioaccessibility. Chemosphere. 2024;352(000).

55. Wang J, Hou Q, Zhang C, Li K, Yang Z, Yu T, et al. Spatial distribution and source apportionment of antimony and arsenic in soil of Dongting Lake Basin, China. Environmental Research. 2026;291(c):123602.

56. Qiao W, Wang Y, He P, Yin X, Zhang D, Bai G, et al. Groundwater arsenic and antimony mobility from an antimony mining area: Controls of sulfide oxidation, carbonate and silicate weathering, and secondary mineral precipitation. Water Research. 2025;273(000).

57. Ferrari C, Resongles E, Freydier R, Meheut M. Antimony isotopic fractionation in the environment: first insights from theorical and experimental investigations. 2021.

58. Zheng J, Liu L, Li Q, Zhao P, Liao Q, Li Q, et al. In situ stabilization of antimony and arsenic in co-contaminated soil using organic matter-Fe/Mn(hydr)oxides colloids and their mineral phase transformation. Journal of Environmental Sciences. 2025(10):835-48.

59. Steven D, Calvin L, Jessica H, Tighe MK, Johnston SG, Milan LA, et al. Speciation and mobility of antimony and arsenic in a highly contaminated freshwater system and the influence of extreme drought conditions. Environmental Chemistry Environ Chem. 2021;18(7):321-33.

60. Zhang P, Xiao J, Yu Z, Liao L, Xiao W, Yuan S. Release and immobilization of arsenic and

antimony in contaminated soil system during sulfidation and reoxidation cycling. Journal of Hazardous Materials. 2010;498(000):11.

61. Gao M, Li H, Xie Z, Li Z, Luo Z, Yu R, et al. The fate of Arsenic associated with the transformation of iron oxides in soils: The mineralogical evidence. Science of The Total Environment. 2024;914(000):10.

62. Pan L, Chen F, Zhao Q, Yang J, Qiu Y, Wu X, et al. Soil antimony–microbe interactions in an abandoned antimony mine in southern China. Environmental Research. 2025;284(c):122268.

63. Yang H, Huang K, Zhang K, Weng Q, Zhang H, Wang F. Predicting Heavy Metal Adsorption on Soil with Machine Learning and Mapping Global Distribution of Soil Adsorption Capacities. 2021.

64. Sun J. Multimethod Analysis of Heavy Metal Pollution and Source Apportionment in a Southeastern Chinese Region. Applied Sciences. 2024;14.

65. Gao S, Wang Q, Poon LCS. Sustainable reuse of modified incineration sewage sludge ash (M-ISSA) for stabilization of highly As-contaminated soil. Journal of cleaner production. 2024;472(Sep.25):1-8.

66. Ma C, Wang M, Li Q, Vakili M, Zhang Y, Hei S, et al. Distribution, source apportionment, and assessment of heavy metal pollution in the Yellow River Basin, Northwestern China. ENGINEERING Environment. 2025;19(2):16-null.

67. Zeng K, Liu L, Zheng N, Yu Y, Xu S, Yao H. Iron at the helm: Steering arsenic speciation through redox processes in soils. Environmental Research. 2025;274(000).

68. Yan H, Wang B, Zheng K, Peng C, Yan J, Qian B. Integrated Analysis of Heavy-Metal

Pollution in Three Gorges Reservoir Sediments: Spatial Distribution, Source Apportionment, and Ecological Risk Assessment. Water (20734441). 2025;17(19).

69. Chebykina E, Abakumov E. Estimation of heavy metals content and regularities of its migration within a soil profile during pyrogenic soil formation in the context of the Scotch pine forest in Togljatty city. Folia Oecologica. 2023;50(2).

70. Taghizadeh-Mehrjardi R, Fathizad H, Mohammad AHA, Sodaiezadeh H, Kerry R, Heung B, et al. Spatio-Temporal Analysis of Heavy Metals in Arid Soils at the Catchment Scale Using Digital Soil Assessment and a Random Forest Model. Remote Sensing. 2021;13(9).

71. Jiao W, Wu M, Hu T, Qi C. Global ecological risk assessment of soil contamination by heavy metal(loid)s based on machine learning. Journal of Environmental Management. 2026;398(c):128435.

72. Lundberg S, Lee SI. A Unified Approach to Interpreting Model Predictions. 2017.

73. Zhou R, Chen J, Cui S, Li L, Qian J, Zhao H, et al. A data-driven framework to identify influencing factors for soil heavy metal contaminations using random forest and bivariate local Moran's I: A case study. Journal of Environmental Management. 2025;375(000).

74. Wang C, Shi M, Wang J, Zhong C. Geochemical characteristics of metal(loid)s in forest soil profiles affected by Pb-Zn ore mining. Journal of Cleaner Production. 2010;501(000):10.

75. Xia F, Zhao Z, Niu X, Wang Z. Integrated pollution analysis, pollution area identification and source apportionment of heavy metal contamination in agricultural soil. Journal of Hazardous Materials. 2024(Mar.5):465.

76. Wu J, Huang C. Machine learning-supported determination for site-specific natural background values of soil heavy metals. Journal of Hazardous Materials. 2025;487(000).

77. Qi C, Li K, Jiao W. Continental-Scale Mapping of Soil Nickel: Integration of Spectral Preprocessing and Machine Learning Approaches. Sustainability (2071-1050). 2026;18(4).